



# On-ground calibration of low gain response for Gamma-Ray Detectors onboard the GECAM satellite

Chaoyang Li<sup>1,2</sup> · Wenxi Peng<sup>2</sup> · Yaqing Liu<sup>2</sup> · Xingzhu Cui<sup>2</sup> · Zhenghua An<sup>2</sup> · Xinqiao Li<sup>2</sup> · Shaolin Xiong<sup>2</sup> · Dali Zhang<sup>2</sup> · Ke Gong<sup>2</sup> · Min Gao<sup>2</sup> · Dongya Guo<sup>2</sup> · Xiaohua Liang<sup>2</sup> · Xiaojing Liu<sup>2</sup> · Rui Qiao<sup>2</sup> · Xilei Sun<sup>2</sup> · Jinzhou Wang<sup>2</sup> · Xiangyang Wen<sup>2</sup> · Yanbing Xu<sup>2</sup> · Sheng Yang<sup>2</sup> · Fan Zhang<sup>2</sup> · Xiaoyun Zhao<sup>2</sup> · Juncheng Liang<sup>3</sup> · Haoran Liu<sup>3</sup> · Zhijie Yang<sup>3</sup> · Xiaofei Lan<sup>1</sup>

Received: 29 April 2022 / Accepted: 22 February 2023 / Published online: 7 July 2023

© The Author(s), under exclusive licence to Springer Nature B.V. 2023

## Abstract

The Gravitational wave high-energy Electromagnetic Counterpart All-sky Monitor (GECAM) consists of two small satellites operating in the same Earth orbit with opposite phases. Its scientific goal is to monitor the electromagnetic counterparts associated with Gravitational Wave events (GWE) and other cosmic high energy transient sources. As the main detector, the Gamma-Ray Detector (GRD) adopts LaBr<sub>3</sub>:Ce scintillator coupled with SiPM array. Each GRD has two output channels, i.e. high gain channel (8 ~ 250 keV) and low gain channel (50 ~ 6000 keV). In this paper, we present the low gain calibration results of GRDs with radioactive sources on ground, including the E-C relation, energy resolution, absolute detection efficiency and spatial response. Meanwhile, the consistency between the measurements and Geant4 simulation demonstrates the accuracy of the simulation code.

**Keywords** GECAM · Gamma-Ray Detector · Energy response · Calibration

---

✉ Wenxi Peng  
pengwx@ihep.ac.cn

✉ Yaqing Liu  
liuyaqing@ihep.ac.cn

✉ Xiaofei Lan  
lan-x-f@cwnu.edu.cn

<sup>1</sup> School of Physics and Astronomy, China West Normal University, Nanchong 637002, China

<sup>2</sup> Key Laboratory of Particle Astrophysics, Institute of High Energy Physics, Chinese Academy of Sciences, Beijing 100049, China

<sup>3</sup> National Institute of Metrology, Beijing 100029, China

## 1 Introduction

GECAM is a space mission dedicated to detect Gamma-ray bursts (GRBs) from celestial bodies, especially those from electromagnetic counterparts of the Gravitational Wave Events. GECAM consists of two small satellites (GECAM-A and GECAM-B) in opposite orbit phases, to achieve an all-sky FOV (Field of View). GECAM has a wide energy range [1, 2], high time resolution [3, 4] and good localization accuracy [5, 6]. The main feature is that once a Gamma-Ray Burst (GRB) is detected by GECAM, the trigger time, source location, and the light curve data can be transmitted simultaneously to the ground station through the BeiDou navigation system.

GECAM is equipped with two kinds of detectors: Gamma-Ray Detectors (GRDs) and Charged Particle Detectors (CPDs) [7]. In the dome cabin of the satellite, twenty-five GRDs and six CPDs are installed evenly, and extra two CPDs are installed in the electronics cabin (Fig. 1 left). GRDs adopt large volume  $\text{LaBr}_3:\text{Ce}$  crystals coupled with SiPM array, and the energy band of gamma-rays is about  $8 \text{ keV} \sim 6 \text{ MeV}$ . CPDs employ plastic scintillators to monitor the flux of charged particles, which is used to help GRDs discriminate the charged particle events. Its energy band for electrons is approximately  $200 \text{ keV} \sim 6 \text{ MeV}$  [8]. The energy and spatial responses of GRDs are crucial not only for the spectral analysis, but also for the localization of GRBs. Generally, we will first perform ground calibrations with discrete energies and incident angles, then a validated Monte Carlo simulation code will be used to generate full-scale response matrices of the GRDs, as we did in the similar mission e.g. the HXMT [9].

The principal design of the GRD and some ground test results can be found in previous papers [10–13], including the high gain calibration for GRDs [14]. In this paper, we just focus on the low gain calibration of GRDs. First we will give a brief introduction of GRD, then introduce the calibration experiments and analysis results. Meanwhile, we also present Monte Carlo simulation for comparison and validation.

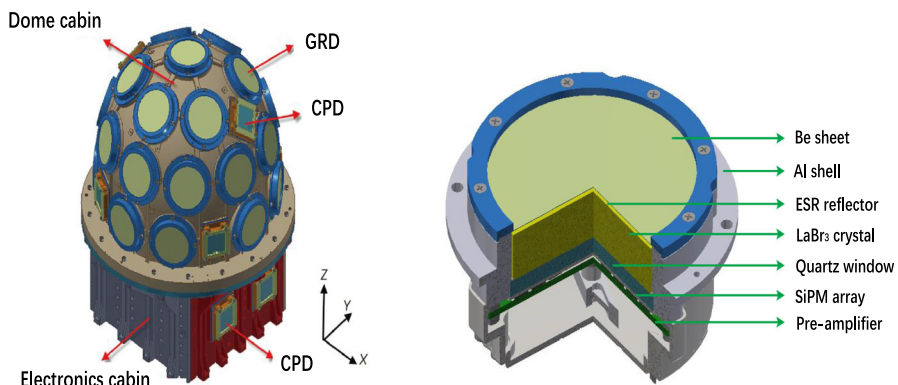


**Fig. 1** Left: The location distribution of GRDs and CPDs on GECAM; Right: The 3D model of GRD

## 2 Instrument description

As indicated in Fig. 1, the GRD is mainly composed of a beryllium window, the LaBr<sub>3</sub>:Ce crystal, a SiPM array and the front-end circuit board. The thickness of the beryllium window is 0.22 mm and its X-rays transmittance is > 65% @5 keV. The LaBr<sub>3</sub>:Ce crystal has high light yield and fast decay time; its dimension is  $\phi 76.2$  mm  $\times$  15.0 mm. An ESR reflector (65  $\mu$ m in thickness) is attached to the top surface of LaBr<sub>3</sub>:Ce, and the lateral faces of the crystal are covered with Tyvek reflective film (to increase the collection of scintillation photons) fixed by 50  $\mu$ m copper tape. The light guide is a quartz window coupled with a SiPM array through optical silicone. The SiPM array has 64 individual SiPM chips with low bias voltage and high quantum efficiency. Each chip has an area of  $6.07 \times 6.07$  mm<sup>2</sup>, and comprised 22 292 pixels (each pixel is sized 35  $\mu$ m). When X-rays or gamma-rays enter the GRD and deposit energy in the crystal, the crystal will yield scintillation photons. Light is collected by the SiPMs and converted into electrical signals. The SiPM signals are amplified by the preamplifier, which has two channels for high gain and low gain. The analog pulses of the two channels are sampling by 12 bits FADCs (40MHz) and processed in FPGA. The dynamic detection range is approximately 8 ~ 250 keV in high gain channel and 50 ~ 6000 keV in low gain channel.

## 3 Calibration experiments and results

### 3.1 Energy calibration

Energy response calibrations of GRDs were carried out with four liquid radioactive sources in a radioactivity laboratory (see Table 1). Each source was sealed in an ampoule bottle ( $\phi=1$  cm), and their activities were well calibrated. As shown in Fig. 2, five customized brackets on wooden stands were used to fix four GRDs and one source. The height of the center of GRD above ground was 82 cm, and the source was at the same height. The distance between the entrance window of each GRD and the source was measured. At the same time, four GRDs could be connected via cables to a data acquisition board, which recorded the signal amplitude and arrival time tag for each

**Table 1** Properties of the radioactive sources used for the energy response calibration

Nuclide	Half-life (d)	Activity (Bq)	Activity uncertainty (%)	Gamma-ray energy (keV)	Relative intensity (%)
<sup>113</sup> Sn	115.09	$6.651 \times 10^4$	3.0	391.698	64.97(17)
<sup>137</sup> Cs	10968.25	$1.993 \times 10^6$	2.0	661.657	85.10(20)
<sup>88</sup> Y	106.626	$9.893 \times 10^5$	2.5	898.042	93.70(3)
				1836.063	99.20(3)
<sup>60</sup> Co	1923.915	$3.504 \times 10^6$	2.0	1173.228	99.85(3)
				1332.492	99.98(6)

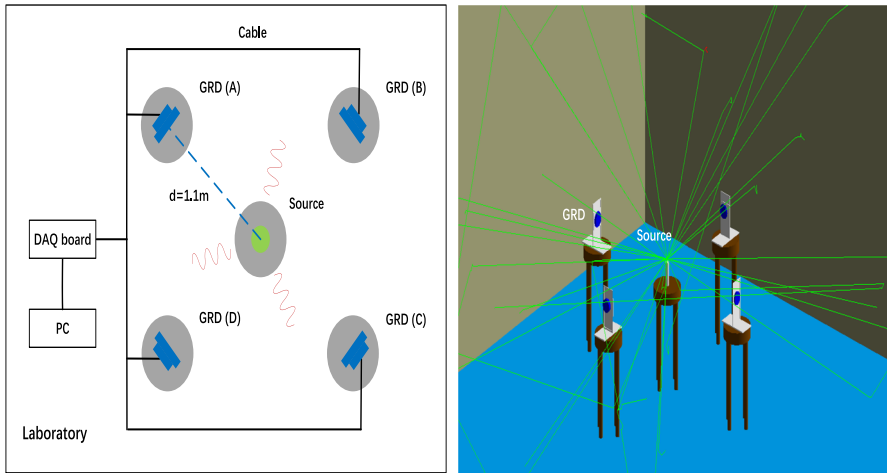


**Fig. 2** Left: Top view of the calibration experiment layout. Four GRDs (A,B,C,D) were measured simultaneously; Right: The Geant4 simulation visualization scene

event. The gain of SiPM was almost stable, because the lab temperature was kept at  $20 \pm 1^\circ\text{C}$ , and the bias voltage was 28 V.

Before setting the source, the background spectrum observed in the laboratory was accumulated for each GRD. As shown in Fig. 3, there are several features in the background spectrum. The first one around 780 keV is due to  $\beta$  particles and  $\gamma$  particles from the intrinsic radioactivity of  $^{138}\text{La}$ . The peak around 1470 keV originates from  $^{138}\text{La}$  and natural radioactivity of  $^{40}\text{K}$  (in the environment) which can be used for gain calibration on ground or in orbit. The bump of three peaks with energy higher than 1470 keV is the contribution of  $\alpha$  particles decayed from  $^{227}\text{Ac}$  and its daughters in  $\text{LaBr}_3:\text{Ce}$  [15].

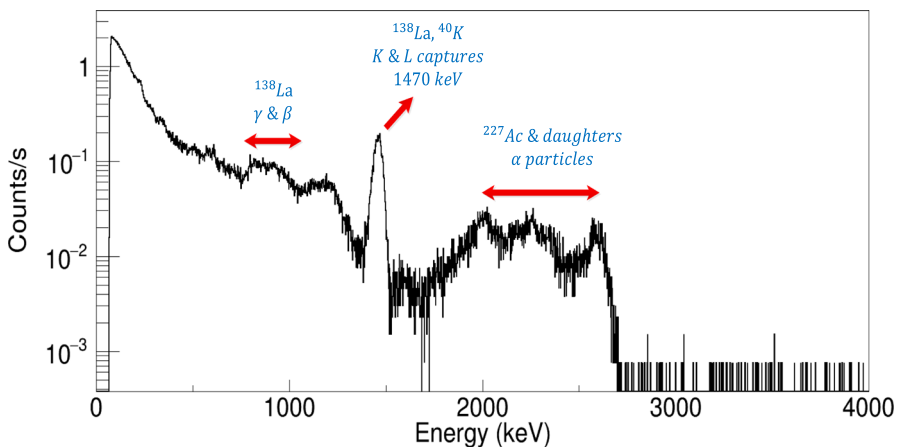


**Fig. 3** The background spectrum of low gain channel

For the measurements with sources, the integration time depended on the source activity and detection efficiency of GRDs. Background-subtracted spectra were then obtained. As shown in Fig. 4, the background-subtracted spectra relative to the various radioactive sources are plotted with solid black curves. Each full-energy peak (solid red curves) was fitted using a Gaussian function (solid blue curves) superimposed on a polynomial function (dotted green curves) [16], which was used to describe the continuum components mainly from Compton scattering. We extracted the fitting parameters, such as the net peak area, the peak position and the FWHM.

We used a linear function to fit E-C relation, i.e. the relationship between the full-energy peak position and the corresponding gamma-ray energies,

$$E = A + B \cdot Ch \tag{1}$$

where  $Ch$  denotes the full-energy peak position,  $E$  is the energy (in keV). Figure 5 (left) shows the fitting result of E-C relation of GRD01 on GECAM-B, and the relative residuals of the fitting are basically within 2%. As shown in Fig. 5 (right), the gains of fifty GRDs have a good consistency within the range of 1.48–1.93 keV/channel. Considering the good linearity of E-C, we can roughly derive the low gain energy range of GRD: 55 keV ~ 5890 keV.

The energy resolution  $R(E)$  is conventionally defined as the FWHM of the pulse-height distribution divided by the position of the full-energy peak [17]. The relationship

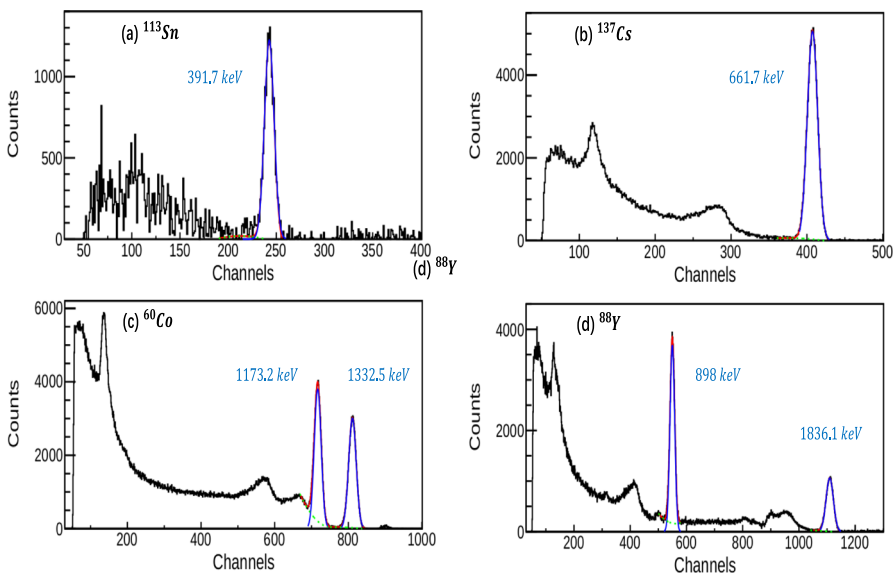


**Fig. 4** Fitting of six gamma-ray lines. The background-subtracted spectra (in black) are plotted. The full-energy peaks are fitted by Gaussian functions (solid blue curves) and the continuum components are in dotted green curves

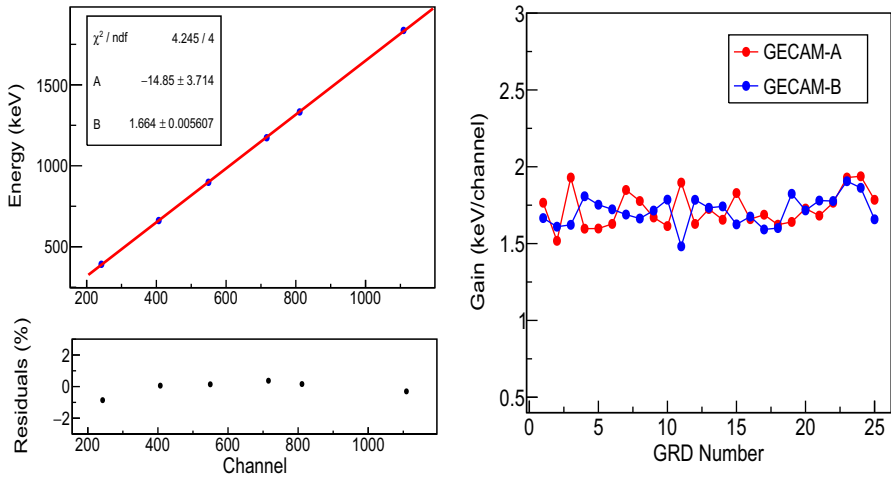


**Fig. 5** Left: The E-C relation of GRD01 on GECAM-B in low gain channel; Right: The gain (keV/channel) of fifty GRDs in low gain channel are compared

between the deposited energy  $E$  and energy resolution  $R(E)$  can be described by the following function,

$$R(E) = \frac{\sqrt{a^2 + (b \cdot \sqrt{E})^2 + (c \cdot E)^2}}{E} \times 100\% \quad (2)$$

where  $a$ ,  $b$  and  $c$  are the fitting parameters. The constant term with parameter  $a$  reflects the electronic noise of the low gain channel. The second term with parameter  $b$  is attributed to the statistical fluctuation of scintillating photons and photoelectrons, and it is proportional to the square root of the deposited energy. The third term with parameter  $c$  represents the non-proportionality of response (nPR) of scintillators, which is proportional to the deposited energy. The fitting results of GRD21 on GECAM-B are shown in Fig. 6 (left) for instance, and the relative residuals are below 3.0%. Here, we also present the energy resolutions of all GRDs, which are in the range of 3.7% ~ 5.3% (@661.7 keV), as shown in Fig. 6 (right).

### 3.2 Spectral response: calibration Vs simulation

Geant4 [18–20] simulations are normally used to generate the full-scale (full energy band and all directions) response for GRDs, and the spectral analysis of calibration can help assess the accuracy of the simulation code. In order to achieve a precise simulation, we reconstructed the experimental environment in Geant4 including not only the GRDs, brackets, wooden stands, but also the walls, cement floor, air (Fig. 2 right) in the laboratory. The GDML model of GRD used in Geant4 [21] was converted directly from CAD model. And *Emstandard\_opt3* was called in Geant4 as a physical list, where photons and charged particles of various electromagnetic interactions with

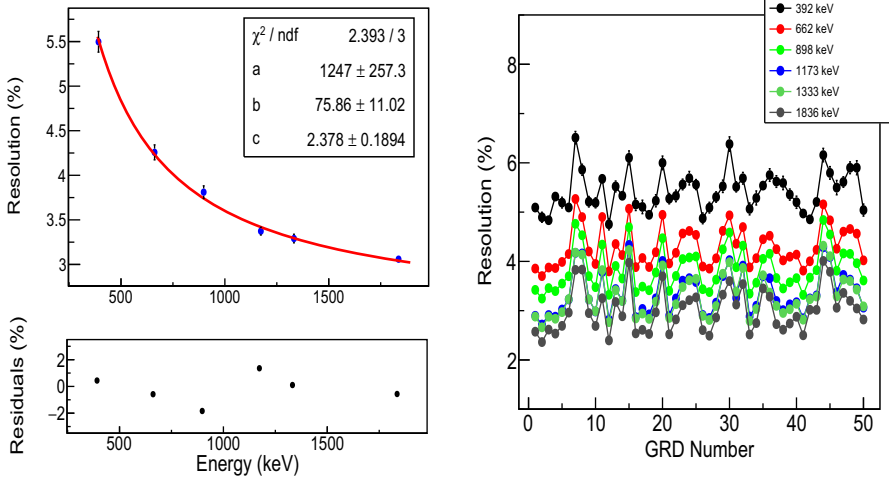


**Fig. 6** Left: The energy resolution and the fitting results of GRD21 on GECAM-B; Right: The low gain energy resolution of fifty GRDs (GECAM-A and GECAM-B)

matter have been registered. For comparison purpose, we utilized the E-C relation to convert channel to energy for the measured spectra (blue line in Fig. 7). Meanwhile, the simulated spectra was broadened according to the measured energy resolution (black line in Fig. 7). As shown in Fig. 7, the simulated spectra are perfectly consistent

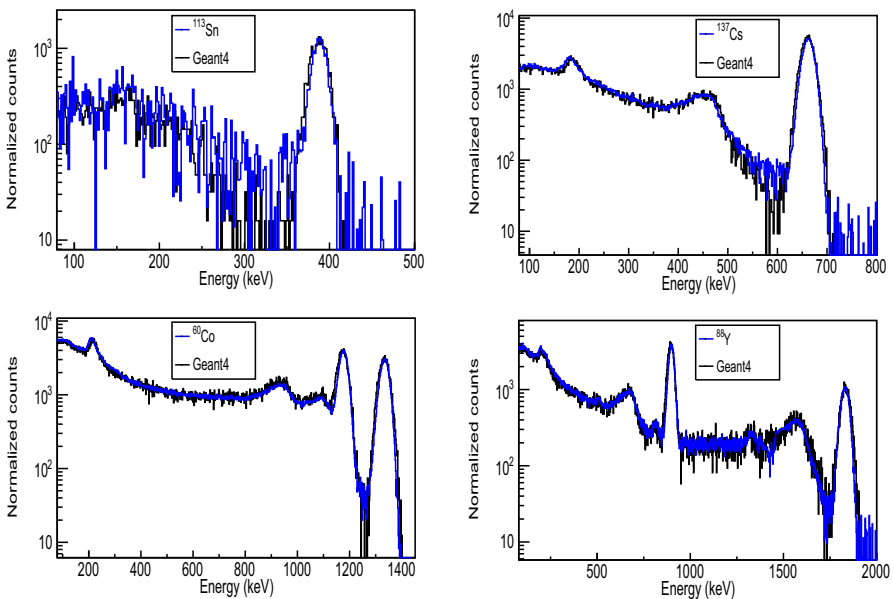


**Fig. 7** The simulated spectra compared with the measured spectra under the irradiation of four radioactive sources

with experimental spectra, including all the features such as the full-energy peaks, the back-scattering peaks, the Compton edges, and the escape peaks. Furthermore, in order to verify the coincidence degree of the two spectra, we implemented a non-parametric test method – Anderson–Darling K (K=2) (ADK) test [22, 23]. For a significance level  $\alpha=0.05$ ,  $p$  value was calculated for each pair of spectra. We got  $p_1=0.54$  ( $^{113}\text{Sn}$ ),  $p_2=0.60$  ( $^{137}\text{Cs}$ ),  $p_3=0.56$  ( $^{60}\text{Co}$ ),  $p_4=0.66$  ( $^{88}\text{Y}$ ), i.e.  $p > \alpha$ , which demonstrated that the simulated spectra and experimental spectra were derived from the same distribution. In another word, our Geant4 code for GRD simulation is reliable.

### 3.3 Absolute detection efficiency

Because the activities of sources were well calibrated (in Table 1), the full-energy peak efficiency of GRD can be calculated as,

$$\varepsilon(E) = \frac{n(E)}{A_0 2^{-t/T_{1/2}} p(E) \omega} \times 100\% \quad (3)$$

where  $n(E)$  is the net full-energy peak area in counts/s;  $A_0$  is the calibrated activity of the radioactive source;  $T_{1/2}$  is the half-life period of source;  $t$  is the elapsed time after the activity calibration;  $p(E)$  is the relative intensity of gamma-rays (listed in Table 1);  $\omega$  is the solid angle ratio of GRD with respect to the source, which has quasi-isotropic emission. Thus  $\omega$  can be described by

$$\omega = \frac{1}{2} \left( 1 - \frac{d}{\sqrt{r^2 + d^2}} \right) \quad (4)$$

here  $d$  is the distance from the beryllium window of the GRD to the source,  $r$  is the radius of the GRD. In Fig. 8, we present the measured full-energy peak efficiencies of several GRDs, which consists with the Geant4 simulation results. The uncertainty on the measured peak efficiency mainly comes from the relative error of the net full-energy peak area (1.6%), the uncertainty of the activity (listed in Table 1) and the uncertainty

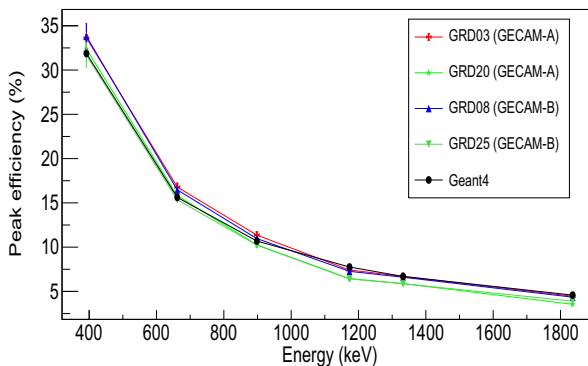


**Fig. 8** The measured peak efficiencies are compared with the simulated peak efficiencies



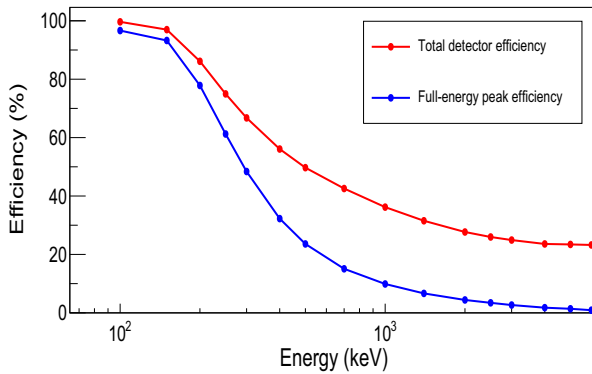


Fig. 9 The full-scale detector efficiency in the low gain simulated by Geant4

of the calculated solid angle ratio (2.0%). Based on simulation, we can further derive a full efficiency curve in the low gain, including full-energy peak efficiency and total efficiency, as shown in Fig. 9. When the incident energy reaches 6 MeV, the total detector efficiency of GRD is still higher than 20%.

### 3.4 Angular response calibration

The GRB localization principle of GECAM is to utilize the relative rates recorded in the GRDs with different orientations to estimate the most likely arrival direction. The energy response and effective area of GRD changes with with the incident angle of gamma-rays. Here, we present the angular response measurement for a single GRD. In this experiment, the GRD was mounted on a customized bracket, which was placed on a rotating platform. The GRD could be rotated in the horizontal plane to change the incident angles (from 0° to 180° with a step of 10°), but the distance between the GRD center and source was kept constant (d=1.07 meter). Figure 10 shows the relative full-energy peak area (normalized to 0°) varied with incident angle at 661.7keV (irradiation

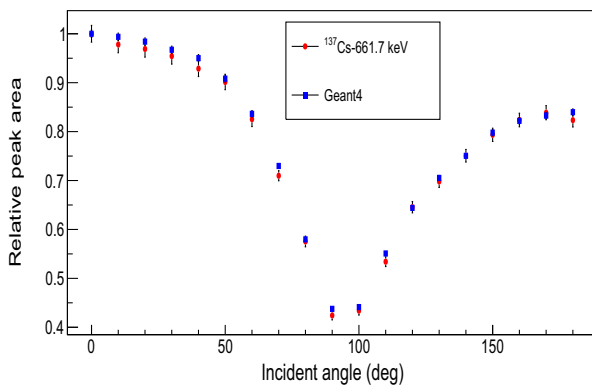
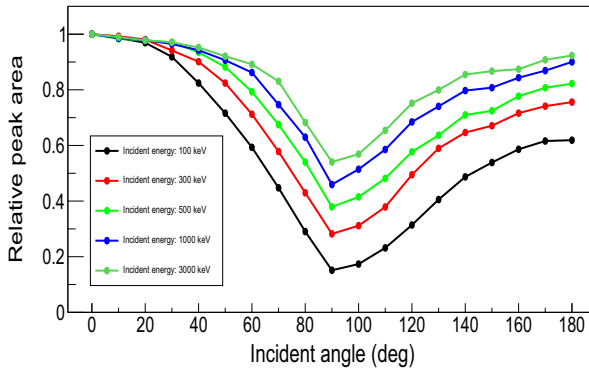


Fig. 10 The relative full-energy peak area (@661.7 keV) Vs the incident angle, normalized to 0°



**Fig. 11** The variation trend of simulated peak area with incident energy and angle, normalized to  $0^\circ$

of  $^{137}\text{Cs}$ ) which are in accord with Geant4 simulation results. The uncertainty on the relative full-energy peak area principally contributed by the relative error of the measured net peak area (1.8%). Based on the simulation, we also present the variation of full-energy peak areas vs. incident angles and energies (normalized to  $0^\circ$ ) in Fig. 11. It's obvious that the peak area is more sensitive to the incident angle at the lower energy, especially for the forward incidence, which implies that the GRBs localization precision will benefit from the measurement of GRD at the low energy.

## 4 Conclusions

In this paper, we investigate the energy response of GRD in the low gain channel via calibration with several radioactive sources and Geant4 simulation. Fifty GRDs have good energy linearity and gain consistency, the energy range of GRDs is approximately 50 keV  $\sim$  6 MeV in low gain channel. The energy resolution at 661.7 keV is in the range of 3.70%  $\sim$  5.27%. Besides, it's good to see that the measured spectra, detection efficiencies and angular responses of GRDs are in accordance with the Geant4 simulation results, which suggests that the Geant4 code of GRD is accurate. Based on an upgraded simulation code (In it, the whole GECAM satellite model was reconstructed), we have produced the energy response matrix of the full energy band with different incident angles for in-flight data analysis.

**Author Contributions** All authors contributed to the study conception and design. W.-X.P. led the calibration experiment design and data analysis. Y.-Q.L. led the experiment setup and data acquisition. Z.-H.A. led the design of GRD. X.-F.L. contributed to the experiment design. S.-L.X. is the P.I. of GECAM. C.-Y.L. led the paper writing. X.-Z.C., X.-Q.L., D.-L.Z., K.G., M.G., D.-Y.G., X.-H.L., X.-J.L., R.Q., X.-L.S., J.-Z.W., X.-Y.W., Y.-B.X., S.Y., F.Z. and X.-Y.Z. contributed to the design and development of GECAM. J.-C.L., H.-R.L. and Z.-J.Y. provided the standard radioactive sources and activity measurements. All authors read and approved the final manuscript.

**Funding** This research is supported by the Strategic Priority Program on Space Science, the Chinese Academy of Sciences, Grant No. XDA15360102, XDA15360300, the National Natural Science Foundation of China (Projects: 12061131007), and the Research Funds of China West Normal University (No. 17E095).

**Availability of data and material** The datasets used and analysed during the current study are available from the first corresponding author on reasonable request.

## Declarations

**Conflicts of interest** The authors declare that they have no conflict of interest.

## References

1. Zhang, D., Li, X., Xiong, S., et al.: Energy response of GECAM Gamma-Ray Detector based on LaB<sub>3</sub>: Ce and SiPM array. *Nucl. Instrum. Methods Phys. Res. A* **921**, 8–13 (2019). <https://doi.org/10.1016/j.nima.2018.12.032>
2. An, Z.H., Sun, X.L., Zhang, D.L. et al.: The design and performance of GRD onboard the GECAM satellite. *Radiation Detection Technology and Methods*, pp 1–10 (2021). <https://doi.org/10.1007/s41605-021-00289-y>
3. Xiao, S., Liu, Y.Q., Peng, W.X., et al.: On-ground and on-orbit time calibrations of GECAM. *Mon. Not. R. Astron. Soc.* **511**(1), 964–971 (2022). <https://doi.org/10.1093/mnras/stac085>
4. Xiao, S., Xiong, S.-L., Wang, Y., et al.: A robust estimation of Lorentz invariance violation and intrinsic spectral lag of short gamma-ray bursts. *Astrophys. J. Lett.* **924**(2), L29 (2022). <https://doi.org/10.3847/2041-8213/ac478a>
5. Jin-Yuan, L.I.A.O., Qi, L.U.O., Yue, Z.H.U., et al.: The localization method of GECAM and simulation analysis. *Sci. Sin.: Phys. Mech. Astron.* **50**(12), 129510 (2020). <https://doi.org/10.1360/SSPMA-2020-0018>
6. Xiao, S., Xiong, S.L., Zhang, S.N., et al.: Enhanced localization of transients based on a novel cross-correlation method. *Astrophys J.* **920**(1), 43 (2021). <https://doi.org/10.3847/1538-4357/ac1420>
7. Li, X.Q., Wen, X., An, Z.H., et al.: The GECAM and its payload. *Sci. Sin.: Phys. Mech. Astron.* **50**(12), 129508 (2020). <https://doi.org/10.1360/SSPMA-2019-0417>
8. Li, C., Peng, W., Xu, Y., et al.: Ground electron calibration of charged particle detectors onboard GECAM satellite. *Nuclear Instruments and Methods in Physics Research Section A: Accelerators, Spectrometers, Detectors and Associated Equipment*, pp. 165969 (2021). <https://doi.org/10.1016/j.nima.2021.165969>
9. Li, X., Li, X., Tan, Y., et al.: In-flight calibration of the insight-hard x-ray modulation telescope. *J. High Energy Astrophys.* **27**, 64–76 (2020). <https://doi.org/10.1016/j.jheap.2020.02.009>
10. Lv, P., Xiong, S.L., Sun, X.L., et al.: A low-energy sensitive compact Gamma-Ray Detector based on LaBr<sub>3</sub> and SiPM for GECAM. *J. Instrum.* **13**(08), P08014 (2018). <https://doi.org/10.1088/1748-0221/13/08/P08014>
11. Chen, C., Xiao, S., Xiong, S. et al.: Design and test of a portable gamma-ray burst simulator for GECAM. *Experimental Astronomy*, pp. 1–14 (2021). <https://doi.org/10.1007/s10686-021-09776-y>
12. Zhang, C., Liang, X., Xu, Y., et al.: Result of proton beam energy calibration of GECAM satellite charged particle detector. *Radiation Detection Technology and Methods*, pp. 1–9 (2021). <https://doi.org/10.1007/s41605-021-00264-7>
13. Zhang, D.L., Gao, M., Sun, X.L., et al.: Quality assurance test and failure analysis of SiPM arrays of GECAM satellites. *Radiation Detection Technology and Methods*, pp. 1–8 (2021). <https://doi.org/10.1007/s41605-021-00282-5>
14. He, J.J., An, Z.H., Peng, W.X., et al.: Ground-based calibration and characterization of GRD of GECAM: 8–160 keV. *arXiv:2112.04787*, <https://doi.org/10.48550/arXiv.2112.04787> (2021)
15. Quarati, F.G.A., Khodyuk, I.V., Van Eijk, C.W.E., et al.: Study of <sup>138</sup>La radioactive decays using LaBr<sub>3</sub> scintillators. *Nucl. Instrum. Methods Phys. Res. A* **683**, 46–52 (2012). <https://doi.org/10.1016/j.nima.2012.04.066>
16. Li, X., Liu, C., Chang, Z., et al.: Ground-based calibration and characterization of the HE detectors for Insight-HXMT. *Journal of High Energy Astrophysics* **24**, 6–14 (2019). <https://doi.org/10.1016/j.jheap.2019.09.003>
17. Tsoufanidis, N., Tsoufanidis, N., Landsberger, S.: *Measurement and Detection of Radiation*. CRC Press, Boca Raton (2019). <https://doi.org/10.1201/9781003009849>

18. Agostinelli, S., Allison, J., Amako, K.A., et al.: GEANT4—a simulation toolkit. *Nucl. Instrum. Methods Phys. Res. A* **506**(3), 250–303 (2003). [https://doi.org/10.1016/S0168-9002\(03\)01368-8](https://doi.org/10.1016/S0168-9002(03)01368-8)
19. Allison, J., Amako, K., Apostolakis, J.E.A., et al.: GEANT4 developments and applications. *IEEE Trans. Nucl. Sci.* **53**(1), 270–278 (2006). <https://doi.org/10.1109/TNS.2006.869826>
20. Allison, J., Amako, K., Apostolakis, J., et al.: Recent developments in GEANT4. *Nucl. Instrum. Methods Phys. Res. A* **835**, 186–225 (2016). <https://doi.org/10.1016/j.nima.2016.06.125>
21. Guo, D., Peng, W., Zhu, Y., et al.: Energy response and in-flight background simulation for GECAM. *Sci. Sin.: Phys. Mech. Astron.* **50**(12), 129509 (2020). <https://doi.org/10.1360/SSPMA-2020-0015>
22. Anderson, T.W., Darling, D.A.: Asymptotic theory of certain “goodness of fit” criteria based on stochastic processes. *The annals of mathematical statistics*, pp. 193–212 (1952). <https://www.jstor.org/stable/2236446>
23. Mantero, A., Bavdaz, B., Owens, A., et al.: Simulation of x-ray fluorescence and application to planetary astrophysics. In: 2003 IEEE Nuclear Science Symposium. Conference Record (IEEE Cat. No. 03CH37515). vol. 3, pp. 1527–1529. IEEE (2003). <https://doi.org/10.1109/NSSMIC.2003.1352167>

**Publisher’s Note** Springer Nature remains neutral with regard to jurisdictional claims in published maps and institutional affiliations.

Springer Nature or its licensor (e.g. a society or other partner) holds exclusive rights to this article under a publishing agreement with the author(s) or other rightsholder(s); author self-archiving of the accepted manuscript version of this article is solely governed by the terms of such publishing agreement and applicable law.